Finite-Element Investigation and Design Recommendations for Perforated Steel Plate Shear Walls

Ronny Purba[1] and Michel Bruneau, F.ASCE[2]

Abstract: This paper presents results from an investigation of the behavior of unstiffened thin steel plate shear wall (SPSW) having a regular pattern of openings (a.k.a. perforated SPSW). Finite element monotonic pushover analyses were conducted, first on a series of individual perforated strips with variation in perforation diameter, to develop a fundamental understanding of the behavior of complete perforated SPSW, then on a corresponding series of complete perforated SPSW having various perforation diameters. Three different sets of wall boundary conditions are considered, namely: flexible beam laterally braced, rigid floor, and rigid beam. Though some differences between the SPSW panel strips and the individual strip results are observed at large monitored strain, at lower monitored strain however the two models are in a good agreement. Based on the analytical results design recommendations of these perforated SPSWs are presented. The shear strength of a SPSW infill plate having a pattern of multiple regularly spaced circular perforations can be calculated as a function of the shear strength of a solid panel, perforation diameter, and distance between perforations.

DOI: 10.1061/(ASCE)ST.1943-541X.0000061

CE Database subject headings: Steel plates; Shear walls; Finite element method; Design.

Introduction

Steel plate shear walls (SPSW) have been rapidly gaining interest in recent years as an effective lateral force resisting system (Sabelli and Bruneau 2007). A key feature of SPSW systems is the significant stiffness and strength they can provide to buildings compared to other lateral force resisting systems. However, in some SPSW applications, the minimum available thickness of infill plate might be thicker such than required by design. Per capacity design principles, at development of the system's plastic mechanism, yielding of the SPSW infill plates will induce relatively large forces to the surrounding frames and consequently will increase the sizes of horizontal and vertical boundary members to which the infill plates are connected. A number of solutions have been proposed to alleviate this concern, either by changing properties of the infill plate via using thin light-gauge cold-rolled (Berman and Bruneau 2003,2005), using low yield strength steel (Vian and Bruneau 2005), introducing vertical slits (Hitaka and Matsui 2003), or introducing multiple regularly spaced perforations, also known as perforated SPSW (Vian and Bruneau 2005). The later solution is appealing as it can at the same time accommodate the need for utility systems to pass through the infill plate, without detrimental effects to the SPSW.

This paper presents the results of an investigation to better understand one aspect of the behavior of unstiffened thin perforated SPSW, more specifically the distribution of yielding around the regularly spaced openings on the infill plate and related requirements to achieve adequate ductile performance, as drift demands relate to infill plate elongations demands. Finite-element (FE) monotonic pushover analysis of subelement (strips) and full specimens are conducted. Based on the analytical results design recommendations and consideration of these perforated SPSW are presented.

[1]Assistant Professor, Dept. of Civil Engineering, Univ. of Bandar Lampung, Lampung 35142, Indonesia (corresponding author). E-mail: ronnypurba@yahoo.com

[2]Professor, Dept. of CSEE, Univ. at Buffalo, Amherst, NY 14260. E-mail: bruneau@buffalo.edu

Note. This manuscript was submitted on March 12, 2008; approved on April 14, 2009; published online on April 16, 2009. Discussion period open until April 1, 2010; separate discussions must be submitted for individual papers. This paper is part of the ***Journal of Structural Engineering***, Vol. 135, No. 11, November 1, 2009. ©ASCE, ISSN 0733-9445/2009/11-1367–1376/$25.00.

Previous Research on Steel Plate Shear Walls

Much research has been conducted since the mid 1980's on SPSW, as summarized in Sabelli and Bruneau (2007). Early studies by Thorburn et al. (1983) introduced the relatively simple Strip model to represent the behavior of unstiffened thin SPSW. Using this procedure, each infill plate is replaced by at least 10 tension strips (of equal width), pin-ended and inclined in the direction of the tension field. This procedure has been demonstrated to generally provide good results (Timler and Kulak 1983; Elgaaly and Liu 1997; Driver et al. 1997). More recently, some researchers have used FE to investigate issues related to SPSWs.

Driver et al. (1997) developed FE models to investigate a large scale, four-storey, single bay unstiffened SPSW having moment-resisting beam-to-column connections and tested by quasistatic cyclic loading. Eight-node quadratic shell elements (S8R5) were used for infill plates directly connected to three-node quadratic beam element (B32) for the beams and columns, omitted the "fish plate" in the model. Initial imperfections of 10 mm based on the first buckling mode of the plate and residual stresses were also incorporated in the FE model. It was found that omitting geometric nonlinearity and second order effects in the FE model caused discrepancy between the cyclic experimental and the analytical results, as pinching of the hysteretic loops was not replicated. Behbahanifard et al. (2003) investigated a three storey specimen created by removing the lower storey of the four-storey specimen tested by Driver et al. (1997). The specimen was tested under

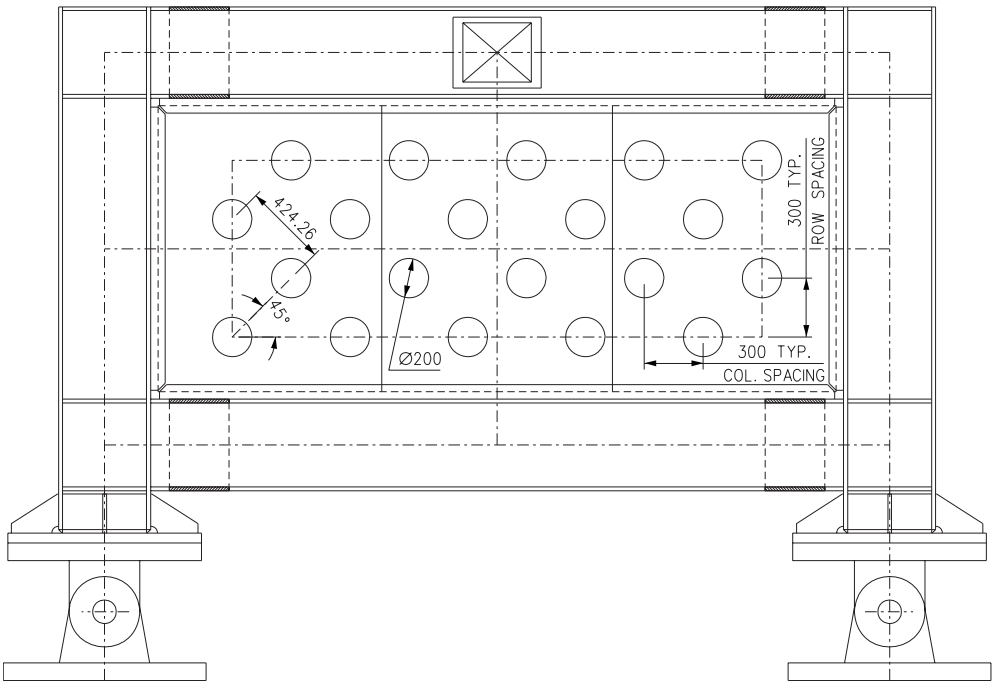

Fig. 1. Perforated SPSW specimen (Vian and Bruneau 2005)

lateral quasistatic cyclic loading in the presence of gravity loads. A nonlinear FE model was developed using ABAQUS/Explicit v. 6.2 to accurately simulate the monotonic and cyclic behaviors of the test specimen. Four-node shell elements with reduced integration (S4R) were used for the entire SPSW. Material and geometric nonlinearity were considered in the FE model. However, residual stresses and plastic deformations from the previous test were not considered due to their complexity. Good agreement was obtained, although the analytical strength underestimated the experimental strength. Both the Driver et al. (1997) and the Behbahanifard et al. (2003) studies focused on SPSW with solid infill plates.

A study on SPSW having single perforations was performed by Roberts and Sabouri-Ghomi (1992). The researchers performed a series of quasistatic cyclic loading tests on unstiffened steel plate shear panels with centrally placed circular openings and recommended that the ultimate strength and stiffness of a perforated panel can be conservatively approximated by applying a linear reduction factor $(1-D/d)$ to the strength and stiffness of a similar solid panel, where D is the hole diameter and d is the specimen width.

Vian and Bruneau (2005) conducted analytical and experimental work on three SPSW to investigate the behavior of specially detailed ductile perforated SPSWs of the type considered in this paper. A first "reference" specimen consisted of a solid infill plate of 2.6-mm thick made of low yield steel with yield stress of 165 MPa framed by 4,000 mm×2,000 mm centerline dimensions with I-shaped sections W18X65 (beams) and W18X71 (columns), and reduced beam sections (RBS) connections. The other two specimens had the same boundary frame, but had staggered holes of diameter 200 mm arranged at a 45° angle with 300 mm center-to-center spacing along both the vertical and horizontal directions on the infill plate, as shown in Fig. 1. A third had reinforced quartercircle cutouts of 500 mm radius at the upper corners of the otherwise solid infill plate. Perforated SPSWs conceptually identical to Vian and Bruneau's second specimen are the subject of this paper. Vian and Bruneau (2005) conducted FE analyses on simplified models to replicate the experimental results. These simplified analytical models were extended to consider various perforation diameters using steel typically specified in North American construction projects. Results illustrated general trends but some erratic jaggedness in the results—Vian and Bruneau's study called for further parametric studies to investigate the causes of the observed variability. This paper undertakes such an investigation, comparing results obtained from individual perforated strip models and full SPSW in terms of structural behavior as well for monitored maximum strain as a function of total strip elongation.

Finite-Element Analysis of Individual Perforated Strip

FE models of individual perforated strips were developed to provide an understanding of their behavior as a fundamental building block in understanding the behavior of complete perforated SPSW. The commercially available software ABAQUS/Standard [Hibbitt, Karlsson, and Sorenson, Inc. (HKS) 2004a,2004b] was used for all analyses in this study. Perforation layout is schemed in Fig. 2 with perforations of diameter D are equally spaced of diagonal width S_{diag}, arranged at an angle θ with respect to the beam axis. A "typical" panel strip defines as the region within a tributary width of $(1/2)S_{\text{diag}}$ on either side of a perforation layout line (Vian and Bruneau 2005), in the figure the region is shaded differently. Typical perforated strips of length L equal to 2,000 mm, diagonal width S_{diag} equal to 400 mm, perforation diameter D ranging from 10–300 mm (corresponding to a perforation ratio D/S_{diag} varying from 0.025–0.75), number of perforations along the diagonal strip N_r equal to 4, and plate thickness t_p equal to 5 mm were investigated (Fig. 3). A perforation diameter increment of 10 mm was chosen for analyses between the limit values of 10

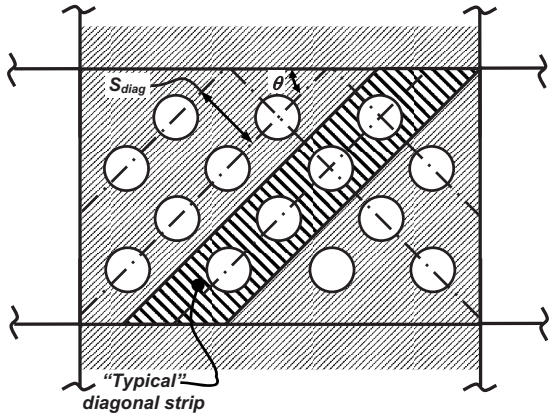

Fig. 2. Schematic detail of perforated SPSW (Vian and Bruneau 2005)

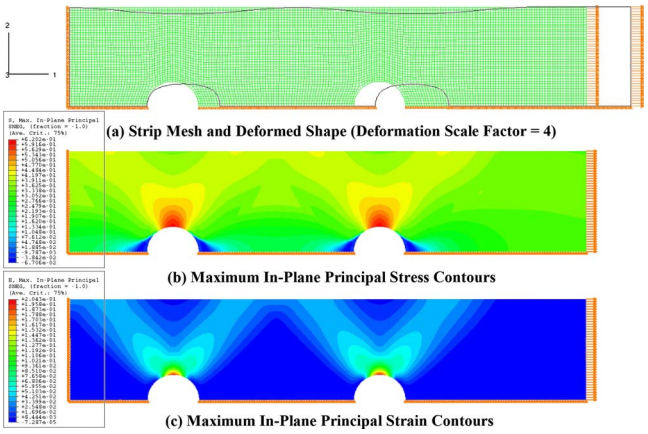

Fig. 4. Typical strip analysis results at $\varepsilon_{max}=20\%$, $D=100$ mm ($D/S_{diag}=0.25$)

and 300 mm, to obtain a relatively large number of data points and thus relatively smooth curves in the plots that express the variation of behavior for various perforation diameters.

Preliminary studies indicated that, due to buckling of the SPSW infill plate, adjacent strips do not affect the stress distribution within an individual strip. Each strip therefore behaves as an independent strip. Results for the full SPSW model presented in a later section will further confirm this postulate. Because the strip geometry and loading are symmetrical about horizontal and vertical axes through the center of the strip, a quadrant of the full-strip is modeled with proper constraints along the symmetric boundaries [Fig. 3(b)]. A monotonic incremental displacement δ was applied to the strip models uniformly along their right-edge until the strips reached a displacement δ equal to 50 mm, or a total uniform strip elongation $\varepsilon_{un}(=2\cdot\delta/L)$ of 5%. During the analysis, total uniform strip elongations were noted when the maximum principal local strain ε_{max} reached values of 1%, 5%, 10%, 15%, and 20% somewhere in the strips.

Isoparametric general-purpose 4-node shell element (S4) was used in the FE models. To investigate the effects of meshing

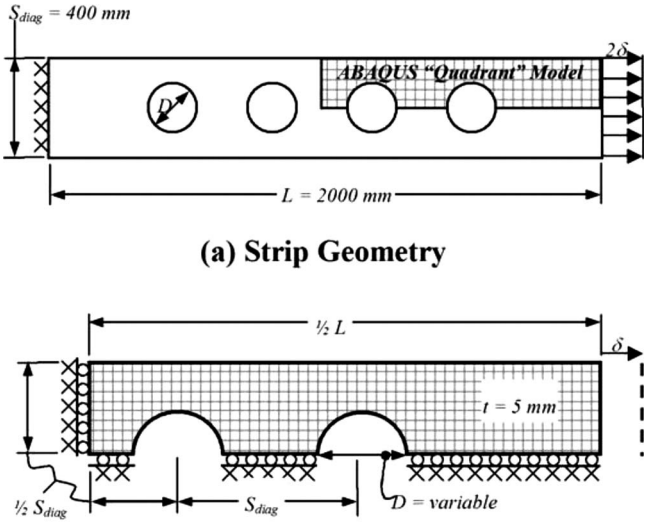

Fig. 3. Individual perforated strip (Vian and Bruneau 2005)

algorithm (transition zones close to the perforations) and mesh refinement on the stress-strain distribution throughout the strips and to ensure a smooth continuity of results, several FE mesh models were developed and analyzed (Purba and Bruneau 2007). As a result, and on the basis of computation time efficiency, a 5 $\times$5 mm mesh size without any transition zone close to the perforations was selected for the parametric study (except that for relatively small and big perforation diameter, i.e., $D\leq 60$ and $D\geq 250$ mm, a rectangular transition zone was used as needed by ABAQUS to mesh the regions close to the perforations correctly, without element distortion).

ASTM A572 Gr. 50 ($F_y=345$ MPa) steel was selected. To investigate how the response of perforated SPSW could be affected by the model assumed for the selected grade of steel, three material models were defined to represent various ways to express the constitutive stress-strain relationship, namely: the idealized trilinear stress-strain model used by Vian and Bruneau (2005), a monotonic uniaxial noncyclic stress-strain, and an elastoperfectly plastic bilinear stress-strain model. The results confirmed the importance of duly modeling strain hardening in the material model to properly capture the spread of yielding needed in this system to allow the strips to reach the total ductile elongation necessary to accommodate the drift demands in perforated SPSW. On the basis of the results, the behavior of steel used was represented by an idealized trilinear stress-strain model.

Behavior of Perforated Strip Model

Fig. 4 shows strip deformations and maximum in-plane principal stress and strain contours at the surface of the shell element for the case having a 100 mm perforation diameter when ε_{max} reached a value of 20% somewhere in the strip. Note that since the high stresses of interest here are tension stresses, results for the center and surface membranes of the shell elements used (S4) were found to be practically identical. As shown in the figure, the in-plane principal stress and strain contours are uniform at the right edge of the strip. However, holes in the strip disturbed the "regularity" of the stress and strain flows and high stress and strain concentrations developed at the perforation edge and zones of yielding radiate out from this location at approximately 45° angles to the left and right of the perforations. In combination with Poisson's-ratio effect, these concentrations also accounted for inward (in addition to rightward) movement of the unre-

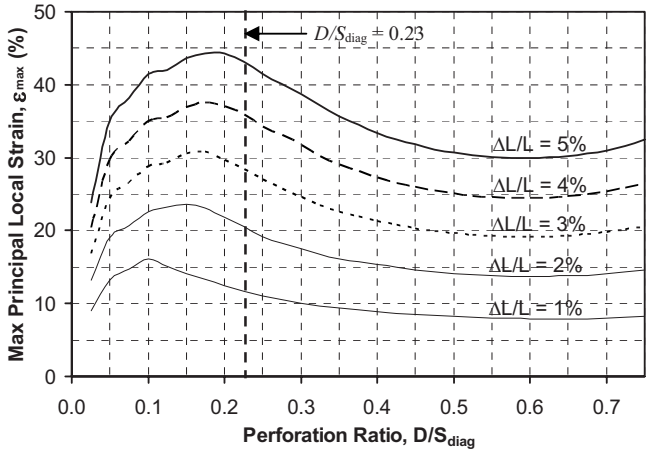

Fig. 5. Maximum local strain ε_{max} versus perforation ratio D/S_{diag}

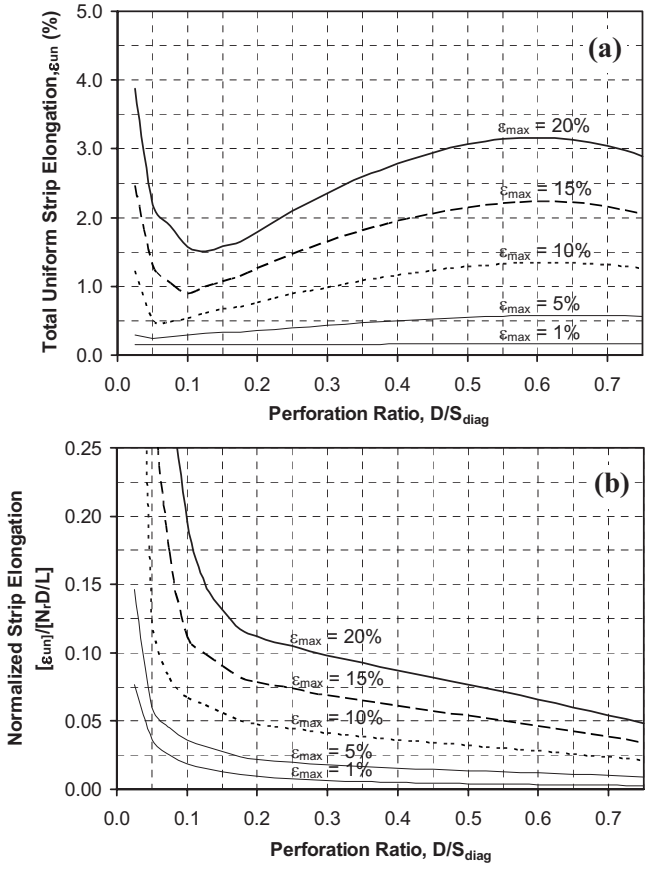

Fig. 6. Strip elongation (a) real value; (b) normalized value

strained top edge (the interface edge to the adjacent strip) adjacent to the perforations. In an actual SPSW, the interface between adjacent strips correspond to a buckle "ridge," and this inward pull toward the hole due to Poisson's-ratio effect would locally reduce the amplitude of the ridge.

As a simple tension member, a more ductile behavior is expected when yielding on gross section precedes net section fracture as the applied axial load is increased (Dexter et al. 2002), i.e.

$$F_u \cdot A_n \geq F_y \cdot A_g \tag{1}$$

where A_n=net strip area; A_g=gross strip area; F_u=ultimate tensile strength; F_y=yield strength. Substituting $A_n=(S_{diag}-D)\cdot t_p$, $A_g=S_{diag}\cdot t_p$, and the properties of A572 Gr. 50 steel used (F_y=50 ksi, F_u=65 ksi) into Eq. (1), the equation can be simplified to $D/S_{diag}\leq 0.23$. This value is used to examine the trend in maximum local strain in the strip for various perforation ratios as plotted in Fig. 5. Note that the increasing and decreasing parts in the figure are roughly separated by the $D/S_{diag}=0.23$ limit.

For the zone where perforation ratio $D/S_{diag}\leq 0.23$, yielding originally occurred in the elements close to the perforation edge and progressively distributed to the gross section as the tensile load increased. As a result and because of strain hardening, the net section has a significant capacity to stretch beyond the point for which the strip has reached the monitored total strips elongation; as the perforation ratio increases, the decreased net section obviously has to stretch more to reach the same monitored elongation. However, for the zone where perforation ratio $D/S_{diag}\geq 0.23$, yielding will be localized to the region close to the perforation while the gross section remains progressively more elastic. By the time the monitored total strip elongation is reached, the shell element close to the perforation edges has reached higher strain and plastic deformation. As perforation diameter further increases, this target limit strain is reached earlier, corresponding to a lesser magnitude of total member elongation. However, note that in SPSW applications even though gross section yielding cannot develop in some cases, the spread of localized yielding, and repetition of it at multiple holes for the perforated plate configuration considered, still make it possible for the perforated plate to reach target total elongations adequate to meet the maximum drift demands for actual SPSW.

Fig. 6(a) presents the effect of holes on strip global deformation where uniform distributed strip elongation ε_{un} versus perforation ratio D/S_{diag} are plotted at 1%, 5%, 10%, 15%, and 20% maximum principal local strain. At higher monitored strain ε_{max} equal to 10%–20%, the total strip elongation decreases significantly at small perforation ratios (i.e., $D/S_{diag}=0.025$ to 0.1 or D=10–40 mm), and then gradually increases between D/S_{diag}=0.1 and 0.6 (D=40–240 mm) before slightly decreasing again for $D/S_{diag}>0.6$. At the lower monitored local strain levels (i.e., ε_{max}=1% and 5%), the total strip elongation remains almost constant for the entire range of perforation diameters.

One might argue that an increase in perforation diameter (for $D/S_{diag}\geq 0.23$) leading to an increase in total strip elongation (for the same monitored local strain) is counterintuitive. For example, to reach a 20% maximum local strain, the strip having a 100 mm perforation diameter ($D/S_{diag}=0.25$) has elongated 21.0 mm ($\varepsilon_{un}=2.10\%$) but the strip with 200 mm perforation diameter strip ($D/S_{diag}=0.50$) elongated even more (as much as 30.7 mm or $\varepsilon_{un}=3.07\%$) before this local strain limit was reached. To explain this behavior, it is first useful to compare the respective area of strip stressed beyond the yield point ($\varepsilon_y=1.725\times10^{-3}$) for the strips having 100 and 200 mm diameter holes. While it was originally suspected that the greater elongation of the strip having 200 mm diameter holes might have been attributed to the longer length over which yielding spread (as a percentage of total plate length), the results actually shows that this is not the case. The area over which inelastic behavior develops (i.e., inelastic area) for the strip having 100 mm diameter holes is larger than that for the strip having 200 mm diameter holes. The percentage of inelastic area over strip net area is about 60% and 43% for the strip having 100 and 200 mm perforations, respectively. Note that these percentages become 58% and 36% if the inelastic area is divided by the gross strip area (i.e., a constant value of 1,000 mm$\times$200 mm=200.000 mm^2 in this case). However, the

magnitude of the inelastic strain develop within these areas of inelastic deformations differs very significantly. One way to capture this difference is by comparing the energy dissipated by plastic deformation for both plates. Even though the inelastic area of the 100 mm perforated strip are bigger than that of the 200 mm perforated strip, its plastic deformation energy (5,530 kN/mm) is smaller than for the 200 mm perforated strip (5,734 kN/mm). This confirms that shell elements close to a bigger perforation edge stretched more than those close to a smaller perforation edge.

To provide additional insight into this behavior, a variation of Fig. 6(a) is plotted in Fig. 6(b) by normalizing the total strip elongation by the factor $N_r.D/L$, which is the ratio of perforated length to overall length in a strip (Vian and Bruneau 2005). Simultaneously, the vertical axis is expressed as $2\cdot\delta/N_r.D$, which is the total strip displacement divided by a total length of perforations over the entire strip. As shown in the figure, for all cases the normalized strip elongation gradually decreases as the perforation ratio increases.

Finite-Element Analysis of Complete Perforated Steel Plate Shear Walls (SPSW)

FE models of complete perforated SPSW (panel models) were developed to verify the appropriateness and accuracy of the individual perforated strip model results and to investigate why prior results from panel analysis in Vian and Bruneau (2005) did not support the predictions from individual strip model analysis. Hence, the same specimen Vian and Bruneau (2005) previously investigated was studied for this objective.

ABAQUS/CAE, a graphical preprocessor program, was used to define the model of the described specimen. Each "plate" of the specimen was modeled independently in its own coordinate system, and using the Assembly Module tools, the parts were then positioned, relative to each other in a global coordinate system, thus creating one final assembly. The fish plate, used in the test specimens to connect the infill plate to the surrounding frame, was not considered in the FE model. Instead, the infill plates were connected directly to the beams and columns, the effects of this assumption to the overall behavior of SPSWs were found to be small (Driver et al. 1997). To avoid distortion, the frame members (beams and columns) were first meshed (using Structured Meshing technique), followed by the infill plate (using Free Meshing technique). As in the strip models, no transition zone close to the perforations was applied except for a small perforation diameter model (i.e., $D=50$ and 100 mm). The meshes started with 50 $\times 50$ mm shell elements near the boundary elements and gradually reducing to an average dimension of 35×35 mm per shell element adjacent to the perforations. The entire infill plate and boundary elements (beams and columns) were meshed using the S4R shell elements isoparametric general-purpose 4-node shell element with reduced integration and hourglass control. ASTM A572 Gr. 50 steel ($E_s=200000$ MPa, $F_y=345$ MPa, $F_u=450$ MPa, and $\nu=0.3$) was selected for boundary elements and infill plate. From case study on material definitions conducted, the unidirectional idealized trilinear stress-strain was appropriate to model the infill plate steel, which can only yield in tension, and immediately buckles in compression. The cyclic stabilized backbone stress-strain curve [equivalent to "Steel A" in Kaufmann et al. (2001) and comparable to the Ramberg-Osgood hysteresis] was used in the boundary elements for the same steel grade.

To help initiate panel buckling and development of tension field action, an initial imperfection was applied to the models analyzed. The shape of the imperfection was a summation of the first 20 modes, each mode having a different amplitude of maximum out of plane deformation, varying linearly from 1 mm for the fundamental mode to 0.01 mm for the twentieth mode. CONN3D2 connector elements were used to model the hinges at the base of the Vian and Bruneau (2005) specimen in the ABAQUS model. This connector links reference nodes at the location of the hinges center, 850 mm below the centerline of bottom beam, to the corner nodes at the tip of each column flange and at the intersection of the flanges and web, and provides effectively a rigid beam connection between two nodes [Hibbitt, Karlsson, and Sorenson, Inc. (HKS) (2004b)]. At the two reference nodes, only rotation about the axis perpendicular to the plane of the wall is allowed, to replicate the hinge rotation in Vian and Bruneau test specimen. The exterior nodes of the flange elements around the perimeter of the panel zones at the top of columns were restrained against out-of-plane movement to replicate the experimental setting of Vian and Bruneau tests. To achieve convergence results without unstable responses due to the higher degree of nonlinearity in the system (infill plate buckling), Stabilize option in ABAQUS/Standard was activated [Hibbitt, Karlsson, and Sorenson, Inc. (HKS) (2004b)]. A monotonic pushover displacement was applied to a reference node located at the middle centerline of the top beam. Fig. 7 shows the resulting FE model. During the analysis, frame drifts and strip elongations were measured (as annotated in Fig. 8) when the maximum principal local strain ε_{max} somewhere in the infill plate reached values of 1%, 5%, 10%, 15%, and 20%.

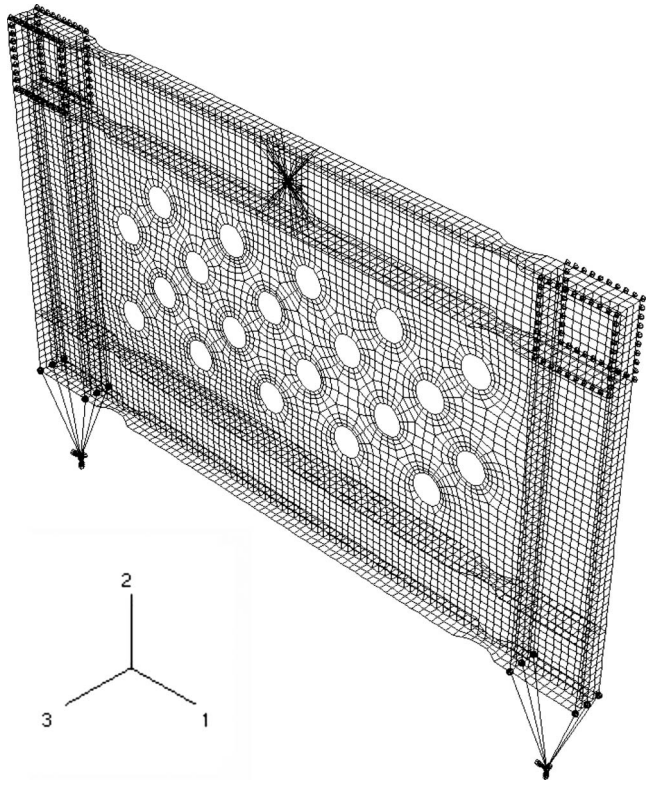

Fig. 7. FE model of perforated SPSW

Behavior of Perforated Steel Plate Shear Walls (SPSW) Considering Alternative Models

At large in-plane drifts, a first model having the boundary conditions described above experienced lateral torsional buckling, pri-

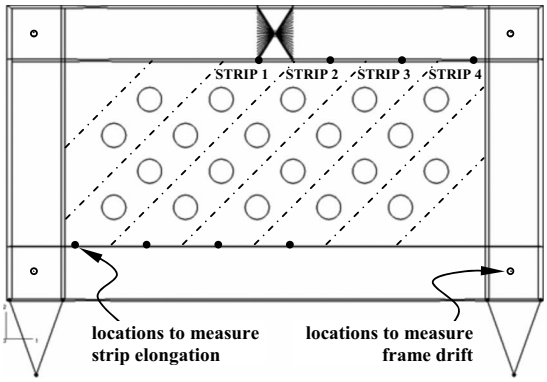

Fig. 8. Strip annotation on perforated SPSW

marily at the top beam and slightly at the bottom beam (not shown here). This phenomenon also affected the columns displacement as the left column deformed in a manner not parallel to the right column. The model was then revised to have lateral supports restraining the out-of-plane movement of the boundary nodes (nodes at the tip of the beams flanges), and called the Flexible Beam Laterally Braced (FLTB) model. In addition, fine meshes were used in this model, starting with 25×25 mm shell elements near the boundary elements and gradually reducing to an average dimension of 15×15 mm per shell element adjacent to the perforations.

For the FLTB model, analysis results showed that every strip reached a different strip elongation. In particular, only Strip 1 matched the individual strip results, while the elongation observed for the other strips in the SPSW panel was less than that for the corresponding stand-alone strip, by as much as 22% for the Strip 4 at 20% maximum principal local strain in the infill plate. The nonsymmetrical beam deflections under the applied diagonal tension from the infill plate caused these deflections and resulting unequal strip axial deformations.

To investigate the significance of beam deformations on strip elongations, the FLTB model was modified by adding vertical constraints at the boundary nodes at the beams flanges (to approximate a rigid-body motion), while all other model properties remained the same, and called the Rigid Floor (RF) model.

For the RF model, the analysis results showed that all strips reached about the same elongation and matched the results obtained for the individual strip model—for example, at monitored strain $\varepsilon_{max} \geq 5\%$, the difference between the results for the two models is less than 2%. Note that the total uniform strip elongation ε_{un} on the tension field strips of a SPSW having rigid pin-ended frame members theoretically can be related to interstorey drift through compatibility relations (Vian and Bruneau 2005) by

$$\varepsilon_{un} = \frac{\gamma_F \cdot \sin 2\alpha}{2} \tag{2}$$

where γ_F=frame (interstorey) drift and α is the tension field inclination angle which is typically forced to be 45° in perforated SPSW. The RF model was developed as a way to approximate (using FE analysis) that theoretical case. The equivalent strip elongation calculated using Eq. (2) for example at 20% ε_{max} consistently closely matched the SPSW strip elongations, i.e., less than 1% difference from the SPSW strips average elongation.

The regularity of the observed deformed shape (Fig. 9), with peaks at the strips lines and valleys between them, illustrates how each strip reached the same elongation. Note that all points along

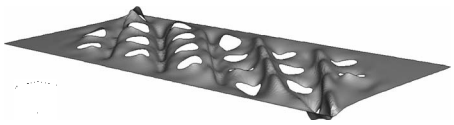

Fig. 9. Infill plate deformation shaped (RF model, deformation scale factor=2.0)

a given peak "ridge" do not reach the same maximum out of plane deformation. Indeed, the magnified deformations shown in Fig. 9 illustrates that the maximum value for the peaks occur along the ridge at the location furthest away from holes, whereas some reduction in the amplitude of the out-of-plane buckle occurs at the point closest to two adjacent holes. This behavior illustrates that the boundary conditions between each individual strip is unrestrained by adjacent strips. As such, each strip behaves as shown in Fig. 3, and the variation of amplitude of out-of-plane deformation along a buckling fold occurs as a result of the reduction of effective width due to Poisson's-ratio effect that develops as the strip elongates.

Note that in the RF model, plastic hinges were constrained to occur in the columns by artificially making the beams infinitely rigid across the entire width of the SPSW. This was done as an interim measure to establish the linkages between full plate behavior and the simplified individual strips. As demonstrated, such a match exists and difference between results for actual unconstrained SPSW and individual strips are primarily due to flexibility of the top and bottom beams, and not some of the other factors (e.g., plate buckling, initial imperfections, etc). To further the understanding of how strip elongations in actual SPSW relate to the individual strip model, an alternative Rigid Beam (RB) model was considered. In this model, a very stiff beam between the RBS is modeled by increasing the thickness of the flanges and webs to be 10 times thicker than for the actual beam. The RBS segments remained at their actual thickness and unconstrained. This allows the rigid-body motions of the beams (translations and rotations) and development of plastic hinges at the RBS connections (as would be expected in correctly designed SPSW).

For the RB model, strips 2 and 3 elongated by almost the same amount reaching 2.75 and 2.69%, respectively, at 20% maximum principal local strain, while Strips 1 and 4 only reached elongations of 2.59% and 2.34%, respectively. This could be attributed to the "kink" that occurred at the RBS connections that are the reference points from which the strips 1 and 4 axial deformations are measured. At lower monitored strain (i.e., $\varepsilon_{max}=5\%$), however, the difference was significantly less since the RBS connections were not severely yielded. Nevertheless, the strips 2 and 3 elongations were 8% and 11% lower than those of their corresponding individual strip, respectively, at the monitored strain $\varepsilon_{max} \geq 10\%$. Effect of mesh refinement was considered and found to insignificantly change these results. Close attention was further paid to the location of ε_{max}.

It was found that when the 20% maximum principal local strain occurred at the "edge" strip, the "full-length" strips reached lower than 20%. Note for the cases considered above, all results were obtained when the target maximum principal local strain was reached at one single location anywhere in the SPSW infill plate, irrespective of where that maximum value was located. It was therefore decided to continue the pushover analysis of the SPSW until one of the "full" strips reached 20% strain next to a perforation. This provided a better match between the SPSW strip results and that of individual strips. It is speculated that maximum

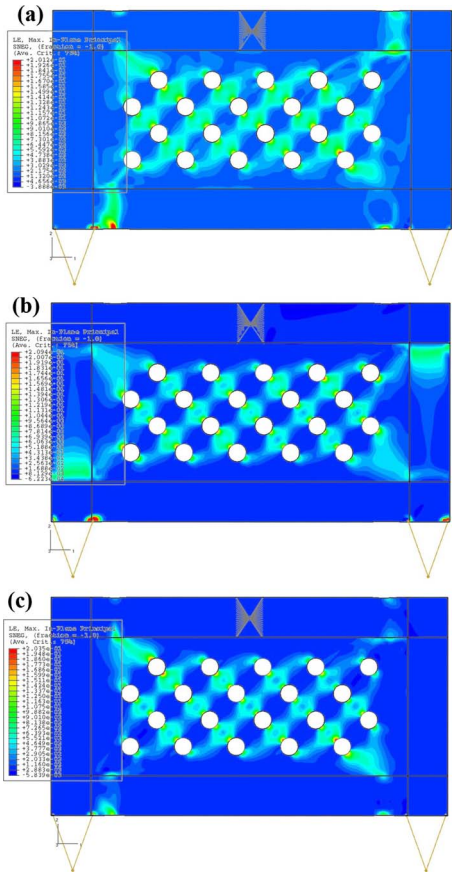

Fig. 10. Typical perforated panel analysis results at $\varepsilon_{max}=20\%$ of (a) FLTB model; (b) RF model; and (c) RB model

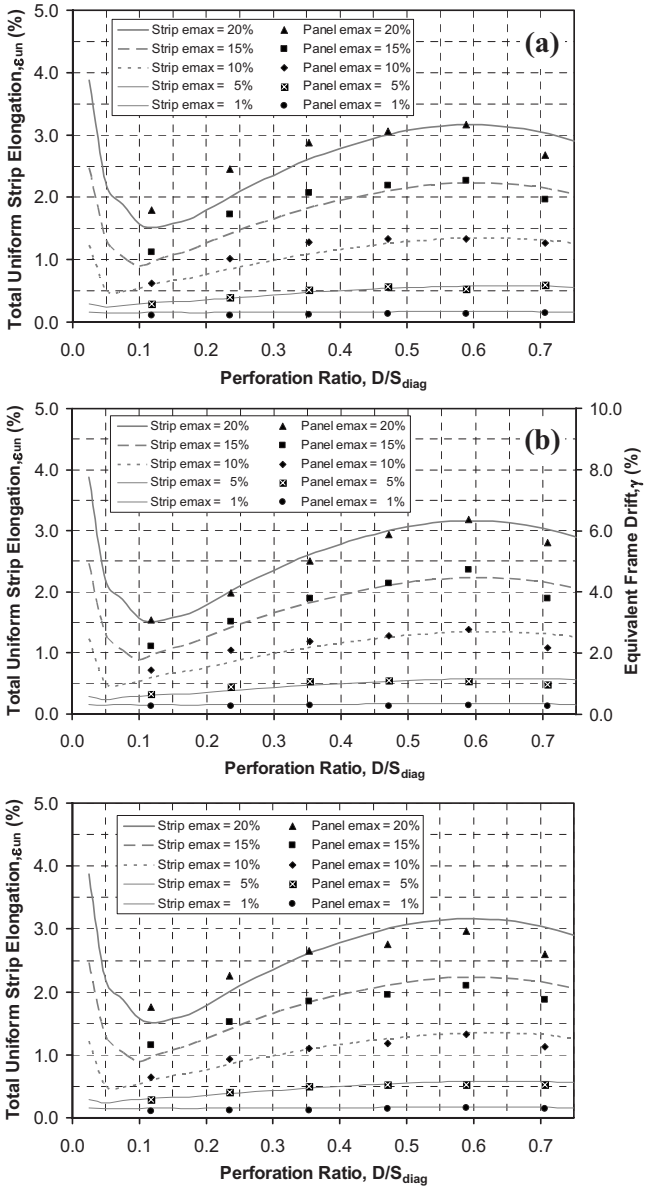

Fig. 11. Uniform distributed strip axial strain ε_{un} versus perforation ratio D/S_{diag} (a) FLTB model; (b) RF model; and (c) RB model

strain occurs in an edge strip due to some combination of biaxial stress condition resulting from constraints at the corner of the plate. Elongation of the RBS flange, compounded with the infill plate elongation, and possibly some artifact due to the rigid beam modeling next to the RBS, may all contribute to this "corner effect." A detailed study of this localized phenomenon is beyond the scope of this study. However, here, results of the original RB model are used and the 15% differences between individual strip results are considered acceptable for all practical purposes.

Fig. 10 presents the in-plane principal maximum strain contours of the three models considered. The distribution of tension field action around the perforations is similar to that observed by Vian and Bruneau (2005). During pushover analysis, yielding was observed to initiate with concentrations at the perforation edges, with zones of yielding radiating out from this location at approximately 45° angles with respect to the diagonal tension field orientation, and then overlapping with yielding zones of adjacent holes from different strips, before finally flowing into the RBS connections (FLTB and RB model) or into the columns (RF model).

Effects of Perforation Ratios and Number of Perforations

To examine the effect of perforation ratios and number of perforations, a series of SPSW using the three analyzed models with perforation diameter $D=50$, 100, 150, 200, 250, and 300 mm was developed and analyzed. This data set allows observation of the trends in SPSW behavior compared to the individual strip results plotted in Fig. 6.

Fig. 11(a) shows the results for the FLTB model. The strip elongation (measured at the strip 2) reached 1.79%, 2.46%, 2.87%, 3.05%, 3.17%, and 2.67% when the maximum principal local strain reached 20% for the respective perforation diameters. Some differences between the SPSW panel strips and the individual strips results are observed at 15% and 20% monitored strain for smaller perforation diameters (i.e., 50, 100, and 150 mm). For example at 20% monitored strain and 100 mm perforation diameter, the differences between the two are as much as 23%.

Fig. 11(b) shows the results for the RF model. Note that since strip elongation can be related to frame drift using Eq. (2) in this case, both strip elongation and frame drift are given on the left and right vertical axes, respectively. As described previously, the RF model having perforated panel with the 200 mm diameter holes matched well the individual strip model results; Fig. 11(b)

further confirms the same result for various perforation ratios. Some insignificant differences occurred at the smaller perforation ratio $D/S_{diag}=0.118$ and 0.236 (which correspond to $D=50$ mm and 100 mm, respectively) at the 5% and 10% monitored strain levels.

Fig. 11(c) shows the results for the RB. The strip elongation (measured at the strip 2) reached 1.75%, 2.26%, 2.65%, 2.75%, 2.96%, and 2.60% to reach a 20% maximum principal local strain for the same respective perforation diameters. Though some differences between the SPSW panel strips and the individual strip results are observed at the 20% monitored strain, at lower monitored strain however the two models are in a good agreement. A less than 15% difference was observed and considered acceptable.

No substantial efforts were invested to investigate why for all models considered, the results for the case with 300 mm perforations ($D/S_{diag}=0.707$) were consistently different from the individual strip results at all monitored strains. In that case, it was found that the zones of yielding propagate more directly from hole to hole instead of radiating out more broadly from the perforation edges in 45° angles as observed for the typical strain distributions plotted in the Fig. 10. However, strain contours of the individual strip at the same perforation ratio exhibited the same yielding pattern so the match between the results should be better. The difference might be attributable to a corner effect of the type previously described and possibly magnified as the size of holes become relatively more significant. Nonetheless, a more detailed investigation of this particular case is beyond the scope of this study.

Panel Strength Design Equation

It had earlier been proposed (Roberts and Sabouri-Ghomi 1992) that the strength of a perforated panel $V_{yp.perf}$ could be conservatively approximated by applying a linear reduction factor to the strength of a solid panel V_{yp}, with same overall dimensions as follows:

$$V_{yp.perf}=\left(1-\frac{D}{S_{diag}}\right)\cdot V_{yp} \tag{3}$$

The proposed equation was developed from a single holed panel. Results of analyses performed with the panel SPSW model were used to reassess the applicability of Eq. (3) for SPSW panels having multiple perforations taking into account the refinements in analysis considered in this study. For comparison purposes, a SPSW having a solid infill panel was also analyzed. This model had the same characteristics as the one used to analyze perforated panels (i.e., material and geometric properties, loading, element type used in ABAQUS, and initial imperfection). For both the solid and perforated SPSW models, the infill panel strength was determined by subtracting the strength of the bare frame (determined from an additional analysis of the boundary frame alone) from the total SPSW strength. Results and discussion are only presented for the RF and RB model.

Fig. 12 presents infill plate strength ratios ($V_{yp.perf}/V_{yp}$) versus perforation ratios (D/S_{diag}) for frame drifts (γ) of 1%, 2%, 3%, 4%, and 5%. Additionally, the predicted value of Eq. (3) is also plotted in this figure (as a solid line). From the two models considered, it can be observed that polynomial regression would provide good correlation with the actual data in developing an equation to predict the strength of the perforated infill plate. For

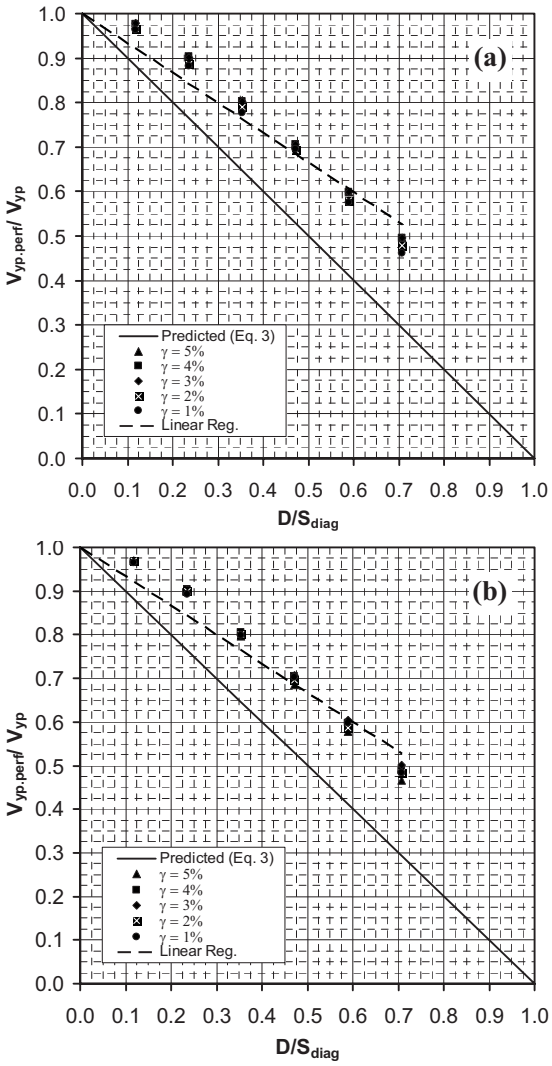

Fig. 12. Infill plate strength ratios ($V_{yp.perf}/V_{yp}$) versus perforation ratio D/S_{diag} (a) RF model; (b) RB model

simplicity, linear regression was applied on a new proposed equation as follows:

$$V_{yp.perf}=\left[1-\alpha\frac{D}{S_{diag}}\right]\cdot V_{yp} \tag{4}$$

where α = proposed regression factor equal to 0.70. In Fig. 12, the results of a linear regression analysis performed on the FE data are plotted as a dotted line. This equation matches within 5% on average the actual data series. This proposed equation is only valid for a wall with a regular grid of uniformly distributed holes covering the entire plate surfaces, as shown in Fig. 1. The equation has been validated for geometries $D/S=0.12$ to 0.71. For example, a wall having a single hole cannot be used using the proposed equation.

It is helpful to illustrate how frame drift correlate to the corresponding local maximum strain in the infill plate for the system considered. Fig. 13 shows this relationship for the RB system. In a design perspective, this figure also provides structural engineers some insight of how high local strain in the infill plate relates to design drift and vise versa. For a selected design drift and for a given perforation diameter, local maximum strain in the infill plate can be determined.

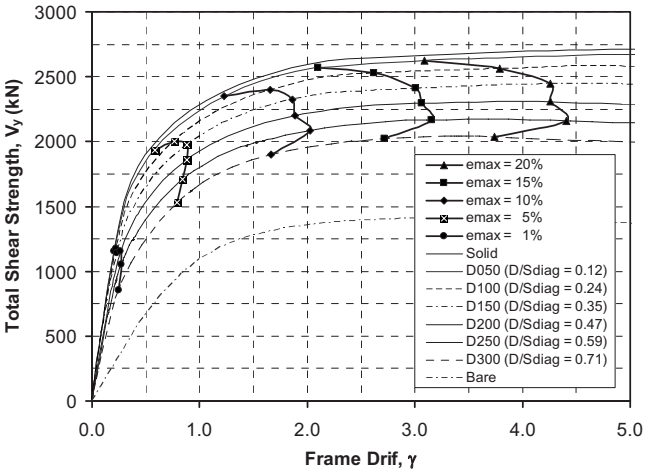

Fig. 13. Total shear strength V_y versus frame drift γ

Design Recommendations and Considerations

Design recommendations for unstiffened thin SPSW having openings are suggested below.

1. The behavior of individual strips can accurately predict the behavior of complete perforated SPSW provided the holes diameter is less than 60% of the strip width. On that basis, if performance of complete SPSW systems with the aforementioned perforation layout is to be evaluated using simpler models, the perforation ratio of SPSW should be limited to $D/S_{\text{diag}} \leq 0.6$, which is a range that should accommodate most practical needs.
2. No interaction exists between adjacent strips that could affect the stress distribution within an individual strip, i.e., each strip in a SPSW behaves as an independent strip.
3. Material properties should model strain hardening to properly capture the spread of yielding in this system needed to accommodate the drifts demands in perforated SPSW.
4. The shear strength of perforated infill plate for SPSW having multiple circular perforations regularly spaced throughout the infill can be calculated by reducing the shear strength of the plate in a solid panel SPSW by a factor $(1-\alpha \cdot D/S_{\text{diag}})$, where α = proposed correction factor equal to 0.70. For panel strength calculated on that basis, the full shear strength of the complete SPSW is conservatively obtained by adding to this value the strength of the boundary frame without the infill.

These design recommendations capture the behavior observed experimentally, and it is recognized that they are limited to the type of regular perforation layout considered here. Future research may allow to investigate other perforation layouts, while providing additional opportunities to validate the proposed design equations.

Conclusions

FE monotonic pushover analysis was performed to investigate the behavior of unstiffened thin SPSW having a regular pattern of openings. Individual perforated strips were first analyzed to develop a fundamental understanding of the behavior of complete perforated SPSW. A series of one-storey SPSW having multiple perforations on panels was then considered, with variation in perforation diameter and boundary conditions. The objective of this analysis was to verify the accuracy of results obtained from FE analysis of individual perforated strips to predict the strength of complete SPSW by summing the strength of "simpler" individual strips. Good agreement in overall behavior between the three models considered and the individual perforated strip model was observed. These models were used to formulate the design recommendations presented in the previous section.

Acknowledgments

Analytical work in this study was performed at the Center for Computational Research at the University at Buffalo, the State University of New York. This work was supported by the Earthquake Engineering Research Centers Program of the National Science Foundation under Grant No. ECC-9701471 to the Multidisciplinary Center for Earthquake Engineering Research. However, any opinions, findings, conclusions, and recommendations presented in this paper are those of the writers and do not necessarily reflect the views of the sponsors.

References

Behbahanifard, M. R., Grondin, G. Y., and Elwi, A. E. (2003). "Experimental and numerical investigation of steel plate shear wall." *Rep. No. 254*, Dept. of Civil Engineering, Univ. of Alberta, Edmonton, Alta.

Berman, J. W., and Bruneau, M. (2003). "Experimental investigation of light-gauge steel plate shear walls for the seismic retrofit of buildings." *Technical Rep. No. MCEER-03-0001*, Multidisciplinary Center for Earthquake Engineering Research, Buffalo, N.Y.

Berman, J. W., and Bruneau, M. (2005). "Experimental investigation of light-gauge steel plate shear walls." *J. Struct. Eng.*, 131(2), 259–267.

Dexter, R. J., Alttstadt, S. A., and Gardner, C. A. (2002). *Strength and ductility of HPS70W tension members and tension flanges with holes*, University of Minnesota, Minneapolis.

Driver, R. G., Kulak, G. L., Kennedy, D. J. L., and Elwi, A. E. (1997). "Seismic behavior of steel plate shear walls." *Rep. No. 215*, Dept. of Civil Engineering, Univ. of Alberta, Edmonton, Alta.

Elgaaly, M., and Liu, Y. (1997). "Analysis of thin-steel-plate shear walls." *J. Struct. Eng.*, 123(11), 1487–1496.

Hibbitt, Karlsson, and Sorenson, Inc. (HKS). (2004a). *ABAQUS/CAE user's manual version 6.5-1*, Hibbitt, Karlsson, and Sorenson, Inc., Pawtucket, R.I.

Hibbitt, Karlsson, and Sorenson, Inc. (HKS). (2004b). *ABAQUS/Standard user's manual version 6.5-1*, Hibbitt, Karlsson, and Sorenson, Inc., Pawtucket, R.I.

Hitaka, T., and Matsui, C. (2003). "Experimental study on steel shear wall with slits." *J. Struct. Eng.*, 129(5), 586–595.

Kaufmann, E. J., Metrovich, B., and Pense, A. W. (2001). "Characterization of cyclic inelastic strain behavior on properties of A572 Gr. 50 and A913 Gr. 50 rolled sections." *Rep. No. 01-13*, National Center for Engineering Research on Advanced Technology for Large Structural Systems, Lehigh Univ., Bethlehem, Pa.

Purba, R., and Bruneau, M. (2007). "Design recommendations for perforated steel plate shear walls." *Technical Rep. No. MCEER-07-0011*, Multidisciplinary Center for Earthquake Engineering Research, State Univ. of New York at Buffalo, Buffalo, N.Y.

Roberts, T., and Sabouri-Ghomi, S. (1992). "Hysteretic characteristics of unstiffened perforated steel plate shear panels." *Thin-Walled Struct.*, 14, 139–151.

Sabelli, R., and Bruneau, M. (2007). *Steel plate shear walls (AISC design guide)*, American Institute of Steel Construction, Inc., Chicago, Ill.

Thorburn, L. J., Kulak, G. L., and Montgomery, C. J. (1983). "Analysis of steel plate shear walls." *Rep. No. 107*, Dept. of Civil Engineering, Univ. of Alberta, Edmonton, Alta.

Timler, P. A., and Kulak, G. L. (1983). "Experimental study of steel plate shear walls." *Rep. No. 114*, Dept. of Civil Engineering, Univ. of Alberta, Edmonton, Alta.

Vian, D., and Bruneau, M. (2005). "Steel plate shear walls for seismic design and retrofit of building structures." *Technical Rep. No. MCEER-05-0010*, Multidisciplinary Center for Earthquake Engineering Research, State Univ. of New York at Buffalo, Buffalo, N.Y.